

Genetic Algorithms Based Orientation and Scale Invariant Localization of Vehicle Plate Number

G. Abo Samra

Abstract— In this research, an enhancement of a previously designed genetic algorithm is introduced to detect the locations of the License Plate (LP) symbols at any in-plane rotation angle. Consequently, the unify-sort-partition-sort (USPS) crossover operator and the objective distance definition introduced in the original system are generalized to support rotation invariability. In addition, a more efficient implementation is introduced in the design of the chromosome layout and the geometric relationship matrix (GRM) to support fast evaluations and convergence in case of inclined plates and missed symbols. A verification stage has been added to filter out false positives and minimize false negatives. Encouraging results with average accuracy above 98% have been reported for a large dataset of 1500 LP samples having variability in orientation, scaling, plate location, illumination and complex background. Examples of highly inclined LP images were successfully detected proving the ability to detect LPs in emergent conditions such as accidents and crime circumstances.

Index Terms— Genetic algorithms, image processing, image representation, license plate detection, road vehicle identification, sorting crossover, USPS crossover.

1 INTRODUCTION

Automatic license plate recognition (ALPR) is the most important module of Intelligent Transportation Systems (ITS). ALPR is used separately to perform vehicle identification for the purpose of toll payment, parking fee payment, freeway and arterial monitoring systems, detection of stolen vehicles, among others [1]-[2]. ALPR is divided into three main steps: plate detection, character segmentation and character recognition. The accuracy and performance of ALPR is significantly dependent on the first two steps. Numerous researches have been based on the three-step approach (excluding the capturing step because it is done by the hardware input device and the preprocessing step because it is included in the detection step) to solve the ALPR problem [1]-[3]. Text-based and texture-based license plate detection can be considered two-step approaches that start by the segmentation of the license text in the image and then do the character recognition step. The main drawback of these segmentation techniques was their intensive computational demand and sensitivity to the presence of other text such as bumper stickers or model identification [1]. Further differentiation between the license text and other types of text data needs the recognition of each character and based on lexical rules related to the license number format, correct detection can be achieved. Detecting license text and at the same time distinguishing it from similar patterns based on the geometrical relationships between the symbols constituting the license number using GA was our novel approach in [3]. Scale and translation invariability were introduced by defining the geometrical relationship matrix (GRM) that encodes the relative locations and dimensions of the symbols inside the plate number resulting in the GA based localization system in [3]. High accuracy above 98% was achieved in a comparison with one of the state of the

art work [4]. Focusing on GA-based systems used in the solution of the License Plate (LP) detection problem, there were three trails [5]-[7] mentioned in [3]. These GA based solutions tried GA but did not introduce general solutions because of color-and-shape dependency with low accuracy, scale dependency, and sensitivity to other text respectively as stated in [3]. Moreover, none of these GA-based algorithms is orientation independent. The necessity of using GAs in the LP problem can be justified by the various researches published in image registration where the goal is to match two images taken under different geometric, lighting, and sensor conditions [8-15]. The detection of a specific LP with a fixed Vehicle Plate Number (VPN) can be regarded as a special case of image registration when the objective is to find a reference image (template) in a landscape image [12]. On the other hand, detection of an unknown LP with unknown VPN cannot be achieved by most of these image matching and registration techniques since the template image and the unknown plate will have a different pattern for the VPN. Hence, there should be a transformation to a feature space, which is invariant w.r.t to the VPN and/or a machine learning technique such as neural network (NN) to detect any LP with any VPN. Following this approach, a serious trial [16] used GA to randomly select candidate positions of LP windows inside an image and evaluate each window based on a NN fed by the vertical-edge-based statistical features of the window. This technique gave better performance than moving a fixed window sequentially from pixel to pixel in the image but it is neither scale invariance (because of fixed window) nor orientation independent (because of vertical edge based features). A recent study [17] used a GA-based technique similar to [16] but the fitness measured by the NN is based on the histogram of oriented gradients (HOG) features of a fixed size window. Although HOG features are scale invariant and a high accuracy rate is reported (above 98%), the technique is still scale and orientation dependent because of using a fixing size window with horizontal orientation. Moreover, using a neural network based evaluation for the fitness function requires too many positive and negative training samples in case of adaption to another LP

• G. Abo Samra is an associate professor in the Faculty of Computing and Information Technology, King Abdulaziz University-Saudi Arabia (phone 00966-509189962; fax:00966-(02) 6951605;email: gabosamra@kau.edu.sa).

layout or style. The main contribution that distinguishes the system in [3] is the use of only one template to locate the license number based on the geometric layout of its symbols without incorporating the shape of the LP or even its colors. This single-template based solution makes it easy to adapt the system on different LP formats or styles. Although the system in [3] showed great tolerance in the localization process in case of physical and/or perspective distortion, higher threshold values that limit the objective distance (*OD*) between the LP prototype and the unknown LP were needed in case of highly inclined plates which would result in more false positives (FPs). Having a wide range of angles allows the ALPR system to detect LP numbers in emergent conditions in which a person or a police officer takes a picture by a hand-held camera or a mobile phone in crime circumstances. Other conditions concern the images of cars before being flipped or turned over in accidents. Hence, our goal in this research is to introduce rotation independency to the system in [3] through several modifications in the GRM layout, the objective function definition and the crossover operator. Many other changes of the system are introduced for performance enhancement as will be described in the following sections. A complete overview of the modified system that we name GABOSIL-VPN (Genetic Algorithms Based Orientation and Scale Invariant Localization of Vehicle Plate Number) for further referencing is given in Section 2. The image-processing phase is summarized in Section 3. In Section 4, the separated objects filtering phase is summarized. GA modifications are demonstrated in Section 5. The results are presented and discussed in Section 6. Finally, the conclusion is given in Section 7.

2 SYSTEM OVERVIEW

In this research, it is intended to separate the new system into three phases, instead of two to support development of each phase separately. The three phases: image processing phase, objects filtering phase and GA phase are shown in the system flowchart in Fig. 1. Each phase is composed of many stages. The starting stage receives an input color image that is processed in the first two phases to produce the best candidate objects fed to the GA phase. The GA phase searches for the optimum objects sequence that resembles an LP number based on the objective distance between the GRM of the unknown object sequence and the input GRM of the prototype LP symbols.

3 IMAGE PROCESSING PHASE

In this phase, an input color image is exposed to a sequence of four stages to extract a number (*N*) of the relevant 2-D objects that may represent the symbols constituting the LP. These four stages (Color-to-Gray Conversion, Adaptive Binarization, Morphological Operations and Connected Component Analysis (CCA)) are the same as in [3] and will not be described again since there is no change done to them. Fig. 2 (a) shows the output of the adaptive binarization stage and Fig. 2 (b) shows

the output of the CCA stage as rectangle-bounded objects.

4 OBJECTS FILTERING PHASE

This phase includes three stages: aspect ratio filtering, dimensional (or size) filtering and black/white ratio (or extension) filtering. These stages can be carried out separately or combined in one stage. Size filtering is the same as in [3]. Aspect ratio and extension filtering are combined due to the nature of some symbols like '1' and 'I' as will be described in the following section.

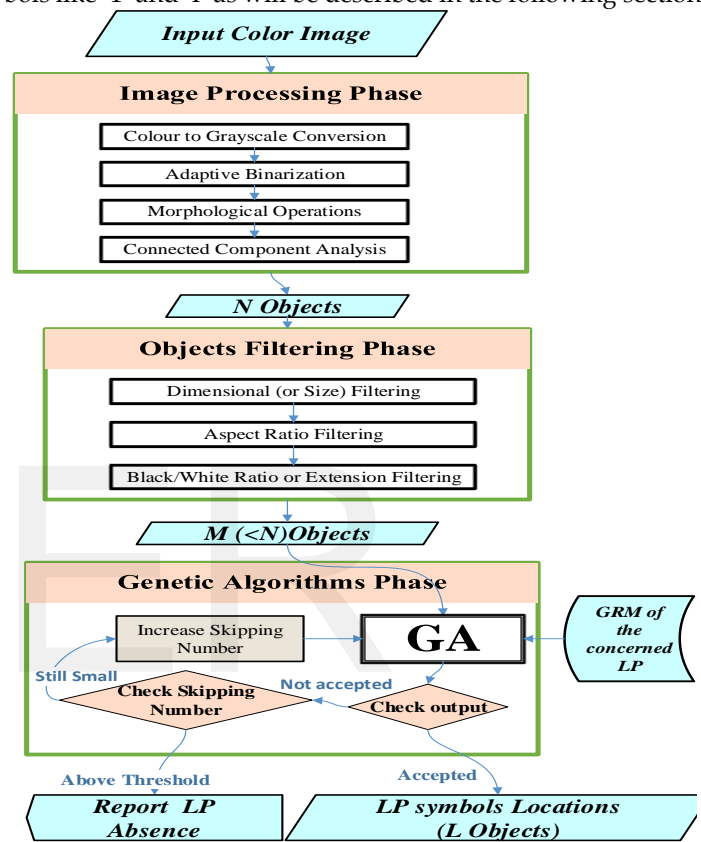


Fig. 1. The system's overall flowchart for the localization of an *L*-symbols LP.

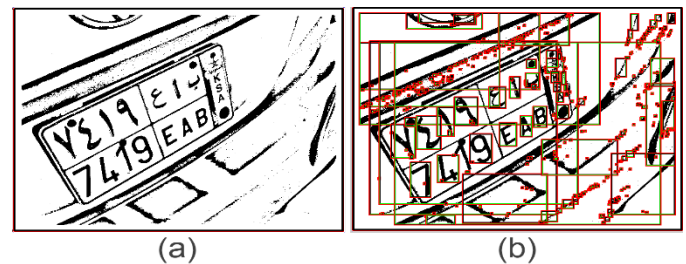


Fig. 2. Image processing stages 2 and 4: (a) Stage 2: Adaptive binarization output. (b) Stage 4: CCA output (440 objects).

4.1 Aspect ratio and extension filtering

Extension filtering is carried out based on the amount of black pixels (*NB*) inside each symbol box that contains other white pixels (*NW*). The extension (*Ext*) is equal to $NB / (NB + NW)$. By measuring the extension of Latin symbols in about 200 Saudi LPs, we found that the extension of license symbols lies between 0.15 and 0.8. We found that the same

range is correct for most Latin symbols present at the public dataset in [18] except for one or two thin symbols such as the digit '1' and the letter 'I'. Hence, by filtering out objects outside the used extension range, a great reduction of the number of output objects is introduced. On the other hand, in most LPs, the box surrounding the LP symbol has an aspect ratio ($ASP=Width/Height$) between 0.3 and 3.3, taking rotation and perspective distortion into consideration. In variable width fonts, some thin symbols like the digit '1' and the letter 'I' may have aspect ratios below 0.3. These thin symbols may also have an extension of 1.0. Hence, the higher limit of extension is not applied on thin symbols leading to the following inequalities for any LP symbol object (obj):

$$0.3 \leq ASP_{obj} \leq 3.3 \text{ AND } 0.15 \leq Ext_{obj} \leq 0.8 \quad \text{for normal symbols} \quad (1)$$

$$(0.05 \leq ASP_{obj} < 0.3 \text{ OR } 3.3 < ASP_{obj} < 20) \text{ AND } (0.10 \leq Ext_{obj} \leq 1.0) \quad \text{for thin symbols} \quad (2)$$

An example of the output of this stage is given in Fig. 3 after applying objects filtering on the objects shown in Fig. 2 (b).

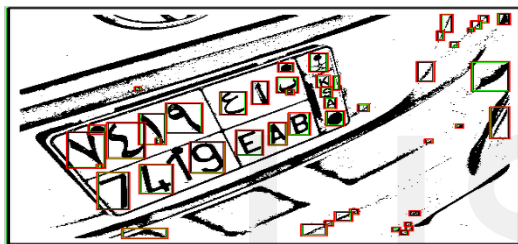


Fig. 3. Output of M (48) objects after objects filtering of the N (440) objects in Fig. 2 (b).

Table 1 gives a real view of the effects of both size filtering and the combined aspect and extension stages for 10 different images; where N is the number of objects output from CCA stage, $M1$ is the number of objects after size filtering only, and $M2(=M)$ is the number of objects after all objects filtering stages.

TABLE 1 NUMBER OF OUTPUT OBJECTS: N (AFTER CCA), $M1$ (AFTER SIZE FILTERING ONLY) AND $M2$ (AFTER OBJECTS FILTERING PHASE) FOR 10 IMAGES.

Img#	1	2	3	4	5	6	7	8	9	10	Average number
N	4576	7544	2034	9119	2628	3812	9518	7885	12662	6392	6617
$M1$	44	63	43	141	38	81	180	118	80	114	90.2
$M2$	40	43	30	134	34	68	163	103	70	101	78.6

5 GA PHASE

Several modifications of this phase have been carried out on the original GA in [3] to support rotation invariability in LP detection. These modifications are done in a smart way in the chromosome layout, genetic operators and objective function to support accurate and relatively fast detection of inclined plates. The details of these modifications will be discussed in the following section.

5.1 Compact chromosome layout

Encoding of the LP is accomplished as in [3] based on the constituting objects inside it taking into account undetected or

missed symbols due to image capturing conditions and image processing problems. An integer-encoding scheme has been selected. The chromosome is composed of L genes. Where L is the number of symbols in the LP. Each gene i is assigned an integer value j , which represents the index to one of the M objects output from the objects filtering phase. The data used for each object j as in [3] are the upper left corner coordinates (x, y) , the height (H) and the width (W) of the rectangle bounding the object. As declared in [3], the Number of Skipped symbols (NS) is set to zero in the first run of the GA. If the objective distance of the best chromosome is above the Objective Distance Threshold (ODT) (or better the maximum allowable objective distance OD_{max}), a new run is initiated after incrementing NS . As shown in the example in Fig. 4 (a), the skipped symbols were represented in [3] by extending the chromosome by a number of genes equal to the maximum allowed number of skipped symbols (4 in case of Saudi LP as set in [3]).

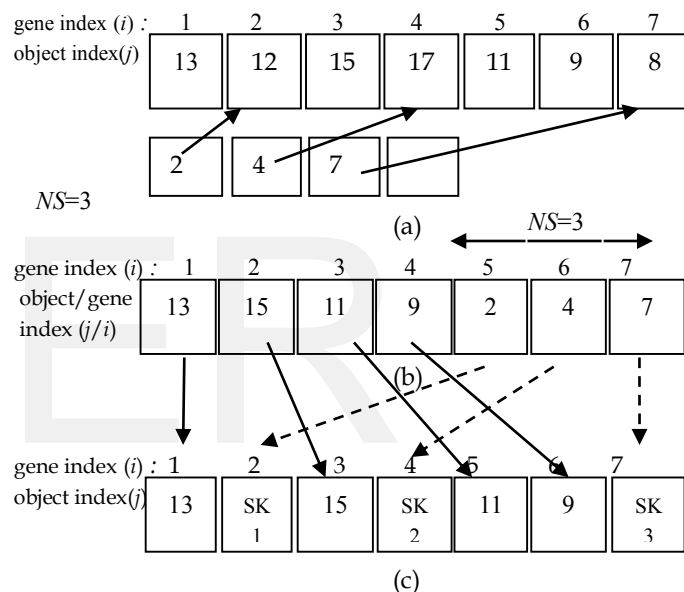


Fig. 4. Original and new layout and mapping steps: (a) Original layout. (b) New layout. (c) The non-skipped symbols in (b) after being mapped to their original locations in the two steps shown by the arrows (step1: dashed arrows and step 2: solid arrows).

Since the skipped symbols indices (j 's) will not be used in any manner and at each run we know their number (NS), hence their locations in the chromosome can be used to store their skipped gene indices (i 's) instead of their object indices (j 's). The NS skipped gene locations are grouped at the tail of the chromosome and their values are initiated as random integers from 1 to L . To illustrate this we refer to Fig. 4 (a), where the skipped symbols locations are 2, 4 and 7 which means that objects 12, 17 and 8 will be considered absent in the current chromosome and their position and dimensional values will not be required in the objective distance calculation. In the new implementation, the skipped gene indices (2, 4 and 7) are stored at the tail of the chromosome as shown in Fig. 4 (b) without extending the chromosome as in Fig. 4 (a). The remaining positions of the chromosome will be just enough to store the $(L-NS)$ non-skipped object

indices and will occupy the front part of the chromosome as shown in Fig. 4 (b). Returning the non-skipped objects to their original positions can be automatically done in two steps when needed as illustrated in Fig. 4 (c). The advantage of this compact representation over the original one lies in saving the positions of skipped symbols which fixes the population representation size to Z (number of chromosomes) $\times L$ integers instead of $Z \times (L+NS)$ integers reducing the search space during skipping and hence decreasing the detection time. Moreover, reaching to the optimum solution will be easier in case of image processing problems such as connection of some symbols to their neighbors or to the plate frame, because these skipped symbols are not fed to the GA and hence it will not wait until other random objects occupy these skipped positions as in the original implementation. Other benefits of this representation exist when doing crossover and mutation as will be shown later.

5.2 Multidimensional GRM Layout

In [3], a 2-D GRM was used to represent the geometric relationships between the consecutive symbols in the prototype LP. The GRM is defined and described in detail in [3].

In short, for L -symbol LP, a $4 \times (L-1)$ matrix was built to represent the geometric relationships between each two consecutive symbols in the LP. The 4 relationships RX , RY , RW and RH are used to represent the relative horizontal and vertical position values and the relative width and height values between each two consecutive objects respectively. Only the relations RX , RY and RH were used in [3] and defined as follows:

$$RX_{i+1,i} = (X_{i+1} - X_i) / H_i \quad (3)$$

$$RY_{i+1,i} = (Y_{i+1} - Y_i) / H_i \quad (4)$$

$$RH_{i+1,i} = (H_{i+1} - H_i) / H_i \quad (5)$$

Since these relationships were stored in the GRM then the calculation of the objective distance in case of no symbol skipping (or in the first run of the GA) is done as described in [3]. In case of skipped symbols, the objective distance is calculated only for the non-skipped objects based on the geometric layout of their corresponding symbols in the prototype plate. This will require evaluation of the relationship values for non-consecutive symbols in the prototype plate such as $RH_{3,1}$ or $RH_{4,1}$ if we skip one or two symbols after the first symbol respectively. Since the GRM matrix is defined for consecutive symbols only, we should deduce the relationships between all non-consecutive symbols to support any skipping case. In general, to deduce the relationship $RH_{i+2,i}$ (by skipping the $(i+1)^{\text{th}}$ symbol) in terms of the stored values of $RH_{i+1,i}$ and $RH_{i+2,i+1}$, then based on (5) we can deduce the following:

$$RH_{i+2,i} = (RH_{i+2,i+1} + 1)(RH_{i+1,i} + 1) - 1 \quad (6)$$

Similarly, based on (3-5) we can deduce that:

$$RX_{i+2,i} = RX_{i+1,i} + (RH_{i+1,i} + 1)RX_{i+2,i+1} \quad (7)$$

$$RY_{i+2,i} = RY_{i+1,i} + (RH_{i+1,i} + 1)RY_{i+2,i+1} \quad (8)$$

Hence, any relationship between non-consecutive symbols can be calculated from the old GRM. Since these relationships are fixed for the prototype plate, we can calculate them at offline and store them in the new layout of the GRM matrix instead of calculating them at runtime. To store the relationships between any two symbols either consecutive or not, the GRM matrix should be a 3-D matrix; where the first dimension refers to the

relation type (1: RX , 2: RY , 3: RH , and 4: RW) and the second dimension refers to the first gene (i_1) which has values from 1 to $L-1$ and finally the third dimension will refer to the second gene i_2 that has values from i_1+1 to L (7 in case of Saudi LP).

In this case, for example, $GRM(1,1,2)$ will contain the value of $RX_{2,1}$ and $GRM(1,1,3)$ will contain the value of $RX_{3,1}$. Also, $GRM(2,1,2)$ will give the value of $RY_{2,1}$ and $GRM(2,1,3)$ will contain the value for $RY_{3,1}$. Having this matrix prepared at start-up of the system will speed up the evaluation of the objective function for each chromosome at run time.

Another step to speed up the calculation of the objective distance is introduced to support rotation invariability in case of inclined plates, by calculating the values of the GRM for the required range of direction angles from $-\theta_n^\circ$ to $+\theta_p^\circ$ after positioning the prototype plate at each angle in this range (instead of mapping each unknown inclined L -objects sequence in the whole population (Z) to the horizontal position). This means that we will have different values for the GRM matrix at different direction angles θ° , which will result in a 4-D GRM matrix represented as follows:

$$GRM(\theta, R, i_1, i_2) \quad (9)$$

Where θ represents the unknown sequence direction angle, R represents the relation type (1: RX , 2: RY , 3: RH , 4: RW), i_1 represents the first gene index, and finally i_2 represents the second gene index where $i_2 > i_1$.

To generate the 4-D GRM matrix we use only one copy of a horizontal plate image as a prototype template. By rotating this template and evaluating the GRM matrix values at each angle starting from $-\theta_n^\circ$ to $+\theta_p^\circ$ we get all relevant values and store the whole GRM into a MATLAB file, which is then loaded at the start-up of the localization program. Adaptation to any new layout will require only the existence of a clear horizontal image of the new prototype including only symbol objects (or better the rectangles surrounding the LP symbols) in their correct horizontal locations without any geometric distortion.

5.3 Objective Distance and Fitness Modifications

The objective distance is calculated as defined in [3], but due to the new compact layout, there should be a type of mapping in case of skipping that should be considered in the evaluation of the objective distance. To clarify this, the evaluation of the RX distance is given as an example. In case of no skipping, the RX distance ($\Delta RX_{k,p}$) between any chromosome k and the prototype chromosome p , corresponding to the input GRM, is defined in [3] as follows:

$$\Delta RX_{k,p} = \sum_{i=1}^{L-1} \left| (RX_{i+1,i})_k - (RX_{i+1,i})_p \right| \quad (10)$$

It should be noted that we mean by $(RX_{i+1,i})_k$ the value of the RX relationship between the object j_1 stored at gene i and the object j_2 stored at gene $(i+1)$ located in the chromosome k ; i.e. there is a hidden mapping from the gene index i to its object index j that is not explicitly shown for simplification. In case of skipping, the skipped symbols are not considered in the objective distance calculations, only the distances between existing symbols and their corresponding ones in the prototype template will be calculated. Hence, there are $(L-NS-1)$ distance values instead of $(L-1)$. If we assume that i refers to the existing symbol gene in the chromosome k , then the corresponding index in the prototype chromosome p may be equal to i or some

other index smaller or greater than i that represents one-to-one mapping from the existing symbol gene index i in the unknown chromosome k to its corresponding one in the prototype p . Hence, there is a one-to-one mapping function, which will be called the skipping map (SkM) that maps each index in the k -chromosome to its corresponding one in the prototype chromosome P . Hence, formula (10) in case of skipping of NS symbols will be rewritten as follows:

$$\Delta RX_{k,p} = \sum_{i=1}^{L-NS-1} \left| (RX_{i+1,i})_k - (RX_{\text{SkM}(i+1),\text{SkM}(i)})_p \right| \quad (11)$$

As an example, SkM of the chromosome in Fig. 4 (b) which has 3 skipped symbols has the following four values: 1,3,5,6.

Another modification that regards the redefinition of the objective distance function in terms of the multi-dimensional GRM is introduced to support invariability with respect to the plate angle. This is accomplished by detecting the main direction of the objects sequence in each chromosome k by averaging the angles made by the vectors connecting each two consecutive objects centers ((CX_i, CY_i) and (CX_{i+1}, CY_{i+1})) with the X -axis as follows:

$$\theta_k = \frac{1}{L-NS-1} \sum_{i=1}^{L-NS-1} \arctan \left(\frac{CY_{i+1} - CY_i}{CX_{i+1} - CX_i} \right) \quad (12)$$

By knowing the chromosome angle θ_k we have two choices:

First, rotation of ($L-NS$) objects for each chromosome in the Z -population by an angle of θ_k to make it parallel to the X -direction. This will take a large computational time because we should rotate the bitmap regions of the objects and scan them pixel by pixel to get the actual positions and dimensions of the boxes surrounding each object after rotation. This processing time can be saved by offline generation of the GRM matrix for the rotated prototype plate symbols at each direction, which is our second choice that has been described in the definition of the constructed multi-dimensional GRM. Hence, formula (11) is rewritten in terms of the GRM matrix defined in (9) as follows:

$$\Delta RX_{k,p} = \sum_{i=1}^{L-NS-1} \left| (RX_{i+1,i})_k - \text{GRM}(\theta_k, 1, \text{SkM}(i), \text{SkM}(i+1)) \right| \quad (13)$$

Due to the variability of the dimensions and positions of the rotated symbols based on their shapes and the angle of rotation, fine-tuning of the weighting parameters (w_x , w_h , and w_y) in the following OD formula defined by [3] is needed.

$$OD_{k,p} = w_x \Delta RX_{k,p} + w_y \Delta RY_{k,p} + w_h \Delta RH_{k,p} + w_w \Delta RW_{k,p} + w_{as} \Delta AS_{k,p} \quad (14)$$

Without rotation we are sure that the relative heights and y -positions between consecutive symbols are fixed (for the Latin part of the Saudi LP and most Latin LPs), but in case of rotation, the relative heights of the symbols and y -positions will vary depending on the symbol's shape as shown in Fig. 5.

In [3], w_h and w_y were given the value of 4 and w_x was given the value of 1. Due to the mentioned variability we did many experiments and found that reducing the values of w_h and w_y from 4 to 3 and increasing the value of w_x from 1 to 1.5, will give better convergence behavior and hence the final objective distance is fine-tuned as follows:

$$OD_{k,p} = 1.5 \Delta RX_{k,p} + 3 \Delta RY_{k,p} + 3 \Delta RH_{k,p} \quad (15)$$



Fig. 5. Change of bounding box sizes of LP symbols due to rotation:

(a) Horizontal plate: all symbols have same bounding box size [159x98], (b) Inclined plate with -40° , different symbols have different sizes Y[163x166], P[138x154], T[163x149], 4[149x137], 0[149x149], 2[170x166], 4[149x137].

Hence, the fitness of a chromosome k (Fit_k) will be given as follows:

$$Fit_k = -1.5 \Delta RX_{k,p} - 3 \Delta RY_{k,p} - 3 \Delta RH_{k,p} \quad (16)$$

In addition, due to the increased variability of the symbol relative positions and dimensions based on the angle of the inclined plate, the threshold OD_{max} is increased linearly with the average angle θ_k as follows:

$$OD_{max} = 4 + 0.1 |\theta_k| \quad (17)$$

The above modifications should decrease the false negatives (FNs) in case of inclined plates but may increase the FPs due to the rising of the objective distance threshold in case of inclined object sequences that may represent fake LPs. Regarding the old system [3], we are sure that both rates will be higher than the new system (GABOSIL) if the old OD_{max} is set to the value that corresponds to the maximum allowable angle in the new system because we increase OD_{max} slightly in the new system based on the inclined angle but it will be fixed at the highest value in [3] for all sequences of objects at any inclined angle.

5.4 The selection method

The Stochastic Universal Sampling (SUS) method has been adopted for the selection of offspring in the new generation as in [3]. Individuals of 80% of the population size ($0.8Z$) are selected to be exposed to mutation and crossover operators with corresponding probabilities $P_c=0.8$ and $P_m=0.02$.

5.5 Mutation operators

In [3], two types of interchangeably used mutation operators have been implemented; substitution operator and swap operator. Due to the new compact layout of the chromosome, the implementation of these operators will be described (taking skipped symbols into account) in the following sections.

1) Substitution operator

In this type of operators, a random position in the chromosome is selected and the corresponding allele is replaced by a new random object from the M available objects if the random position is in the non-skipped region. The new object should be different from other objects in the mutated chromosome. If the random position is located in the skipped region, a new random number from 1 to L substitutes the current value at this random position as in Fig. 6 (a).

2) Swap operator

In this operator, as in [3], we implemented the reciprocal exchange mutation that selects two genes randomly and swaps them as shown in Fig. 6 (b). Swapping in the skipped part has no effect since the order is not important in this part.

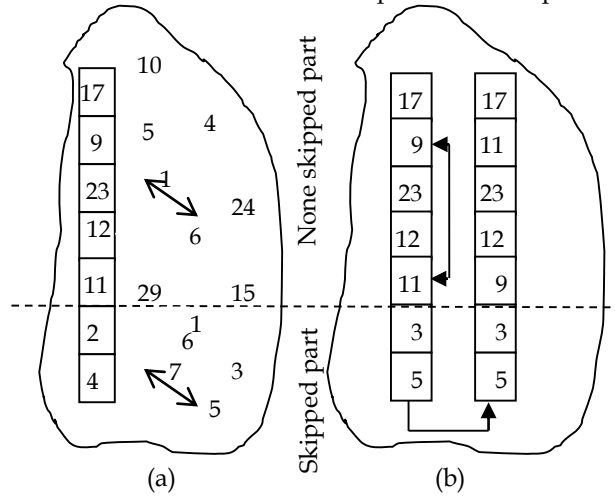


Fig. 6. Examples for the used mutation operators: (a) Substitution operator, (b) Swap operator.

5.6 Unify, Rotate, Sort, Partition, and Sort crossover operator (URSPS)

In [3], the USPS crossover operator was introduced and its capability was experimentally proven by resulting in fast partitioning of objects in parent chromosomes based on their *y*-coordinates (or *x*-coordinates in the alternate operator) to produce more fit offspring. In this work, this operator will be enhanced to perform better in more complex situations of the parent chromosomes such as those shown in the left most and right most cases in Table 2.

TABLE 2 PLATES INCLINED BY DIFFERENT ANGLES AND THE CORRESPONDING ODS WHEN MEASURED BY [3] WHERE THE VERTICAL AND HORIZONTAL BLACK-AND-WHITE LINES SEPARATE THE OUTLINED SYMBOLS EQUALLY.

Image					
θ	- 3 0 °	- 2 0 °	1 0 °	2 0 °	4 5 °
OD	16.6	11.2	06.4	11.2	19.2

Although all the shown LP numbers have been detected using the USPS operator, we have shown that ODmax should be increased in [3] to detect high sloped plates as shown in the left most (-30°) and the right most (45°) plates. This rising of the objective distance threshold, if fixed in [3], will increase FPs and still we will get more delay in the detection time because of the following:

If we assume that the two parents having a mixture of the Arabic and Latin symbols as follow:

$$P1 = |0 |6 |7 |5 | \wp | \wp | \wp | \wp |$$

$$P2 = |6 |5 |0 |7 |T |J |J |B |$$

If we apply the USPS on the plates having angles from -18° to +19°, the two offspring will get the required separated genes. On the other hand, it will be difficult to separate the Arabic and Latin symbols outside the mentioned angle range because of the overlapping of both sequences in both *X* and *Y* directions. For example in case of the 45° rotated plate, after applying the US(*y*)PS(*x*) operator we will get the following offspring:

$$Ch1 = |0 | \wp | \wp |T | \wp |J |B |$$

$$Ch2 = |6 |5 |6 |7 |5 |7 |0 |$$

If we apply the alternate US(*x*) PS(*x*) we will get a similar result. Where we mean by *S*(*x*), sorting based on *x*- coordinates and by *S*(*y*), sorting based on *y*-coordinates. Hence, to reach to the required result by applying the original crossover we will need more generations to separate the Latin part of the license number based on the random distribution of objects inside other chromosomes in the same population and sure, it will require further mutation operations. This problem is not pertinent to bilingual or two-line LPs only but it exists in single line licenses as shown in the 2nd and 3rd rows of the Appendix Table because of overlapping with other objects such as vehicle model or bolts and nails. The overlapping problem can be solved by introducing the rotating URSPS operator, which unifies the two parents and then sorts them based on the vertical distance from an inclined (rotated) axis with random direction that represents a rotated *X*-axis (*X_r*). Since this reference line *X_r* passes through the origin point (0, 0), then its equation can be written as follows:

$$X_r = m_x x \tag{18}$$





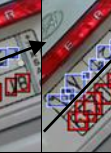
The vertical distance *Y'* between any object *j* at position (*X_j*, *Y_j*) and the reference line *X_r* will be:

$$Y' = Y_j - m_x X_j \tag{19}$$

By giving *m_x* a random value between -tan (θ_n) and +tan (θ_p) and sorting the unified chromosome objects based on *Y'*, the GA will be able to separate symbols of plates inclined with angles from - θ_n to + θ_p . Reported values of the slope *m_x* and the new objective distances after applying the modified operator on the same images in Table 2 are shown in Table 3. The complete steps for the implementation of the URSPS crossover (considering skipped symbols) when applied on the two parent objects shown in Fig. 7 are presented in Fig. 8. From Fig. 8, we notice that the crossover process for a non-zero value of *NS* will be the same as for zero value except that (*L-NS*) genes from each parent are to be recombined instead of *L* genes. In addition, each offspring will take its original skipping values at the end of the crossover operation. Fig. 9 shows convergence graphs for two different LP images (A1 and A2) using the new URSPS at the top graphs (B1 and B2) and the old USPS at the bottom ((C1, D1) for A1 and (C2, D2, E2) for A2).

Regarding the first image (A1), the GA with the old USPS crossover failed in the first run with *NS*=0 (C1) and found the solution at the second run with *NS*=1(D1) where (*L*-1) symbols can be separated as indicated by the Vertical Separating Line (VSL) using the alternate operator US(*x*)PS(*x*) which partitions the objects based on the *x*-coordinates.

TABLE 3 THE SLOPE VALUES (M_x) AT WHICH LATIN AND ARABIC LP-SYMBOLS SHOWN IN TABLE 2 ARE SEPARATED WITH THEIR CORRESPONDING OD_s IN GABOSIL-VPN SYSTEM.

Image	m_x	OD
	-0.50	3.90
	-0.32	3.00
	0.21	1.96
	0.40	2.60
	1.00	3.19

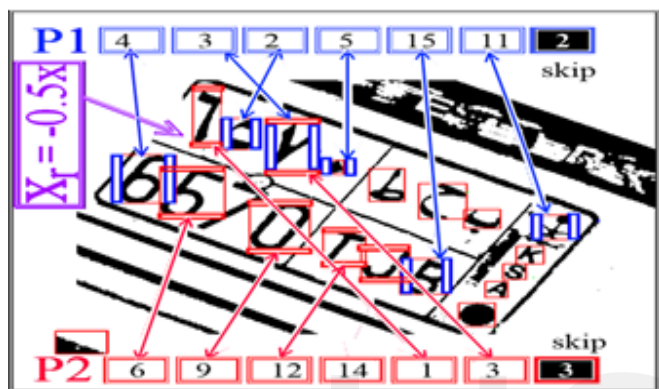


Fig. 7. Parent objects p1 (vertical double lines boundary) and p2 (horizontal double lines boundary) used as inputs to the crossover steps in Fig. 8.; where X_r represents the reference line used in step 2 in Fig. 8.

Considering the second image (A2), the GA with the old USPS crossover failed to find the solution at the first and second runs (C2, D2) and the solution was found randomly at the third run with $NS=2$ (E2) because the overlapping is very high between the Latin and Arabic sequences and at least 3 or 2 symbols are needed to be skipped to allow horizontal or vertical separation as indicated by the VSL or Horizontal SL (HSL) respectively. Without forgetting to compare with random crossover operators, a 2-point random crossover has been modified as in [3] to prevent unaccepted object repetitions and tried for the two test images. The 2-point random crossover found the solution for the first image A1 ($M=333$) at the fourth trail ($NS=3$) after 188 generations whereas it found the solution for the second image (A2) at the second trial ($NS=1$) after 35 generations because of small M ($=20$). Hence, we conclude that the new URSPS operator outperforms both the original USPS and the 2-point random crossovers when detecting highly inclined plates. Considering slightly inclined plates ($|\theta| < 15^\circ$), it was shown experimentally in [3] that the USPS operator outperformed the 2-point random crossover operator. More experiments will be performed to demonstrate the significance of the URSPS operator in the results section.

5.7 Replacement strategy

As in [3], the best 20% of the parents are selected and appended to the offspring (80%) to produce the new generation (100%).

5.8 Stopping criteria

The GA stops if one of the following conditions is met:

1. The best chromosome's objective distance (OD_{best}) is less than the minimum objective threshold (OD_{min}).
2. OD_{min} is decreased in case of skipped symbols by a factor of $((L-NS)/L)$ as a penalty for non-complete matching while it is increased linearly with the absolute value of the average angle of the best chromosome $|\theta_{best}|$ to compensate for the increased OD in case of plate rotation as described before. Hence, the formula for OD_{min} becomes as follows:
3. $OD_{min} = 2 \left(\frac{L-NS}{L} \right) + 0.1 |\theta_{best}|$ (20)
4. OD_{best} is not improved for 5 successive generations and is less than OD_{max} which is given by (17) and modified in case of skipping as follows:
5. $OD_{max} = 4 \left(\frac{L-NS}{L} \right) + 0.1 |\theta_{best}|$ (21)
6. The average objective distance (OD_{av}) is not improved for 6 successive generations.
7. The number of generations N_{gen} reaches to the maximum number of generations $MaxN_{gen}$ (set to 20).

If stopping happens due to reasons 3 or 4, the solution is accepted if OD_{best} is less or equal to OD_{max} .

5.9 Parameters setting

The population size (Z) is selected dynamically as in [3] but after changing 1.65 to 2 to simplify the process of sub grouping (if needed for parallel processing or other reasons) in future developments as follows:

$$Z = 2 \times 2^{(0.21 * \text{length})} \quad (22)$$

Where length is given by:

$$\text{length} = L \times \text{Log}_2(M) \quad (23)$$

5.10 Fake detection and verification stage

Due to the high values of OD_{max} at large angles, some fake outputs are enabled at some cases in the preliminary test of the new system, which necessitates an addition of a fake detection and verification stage. In this stage, if the candidate solution output from the genetic stage has an angle more than 5° and OD_{best} is more than 4.5, the output symbol sequence is rotated with the same angle to be horizontal and the objective distance is recalculated based on the horizontal template producing the horizontal objective distance (HOD). Hence, the output of the GA is accepted if the following logic expression is true:

$$(HOD \leq 3.5) \text{ OR } (OD_{best} \leq OD_{max} \text{ AND } HOD \leq 4.5) \quad (24)$$

Otherwise, the solution is rejected and a new run of the GA stage is initiated with the incremented value of NS . The significance of this stage will be demonstrated in the next section.

6 RESULTS AND DISCUSSION

To evaluate GABOSIL, we collected 466 images in addition to the 800 images used in the first experiment in [3] and generated another 234 images by rotation of different images with various angle values reaching to a size of 1500 LP image dataset.

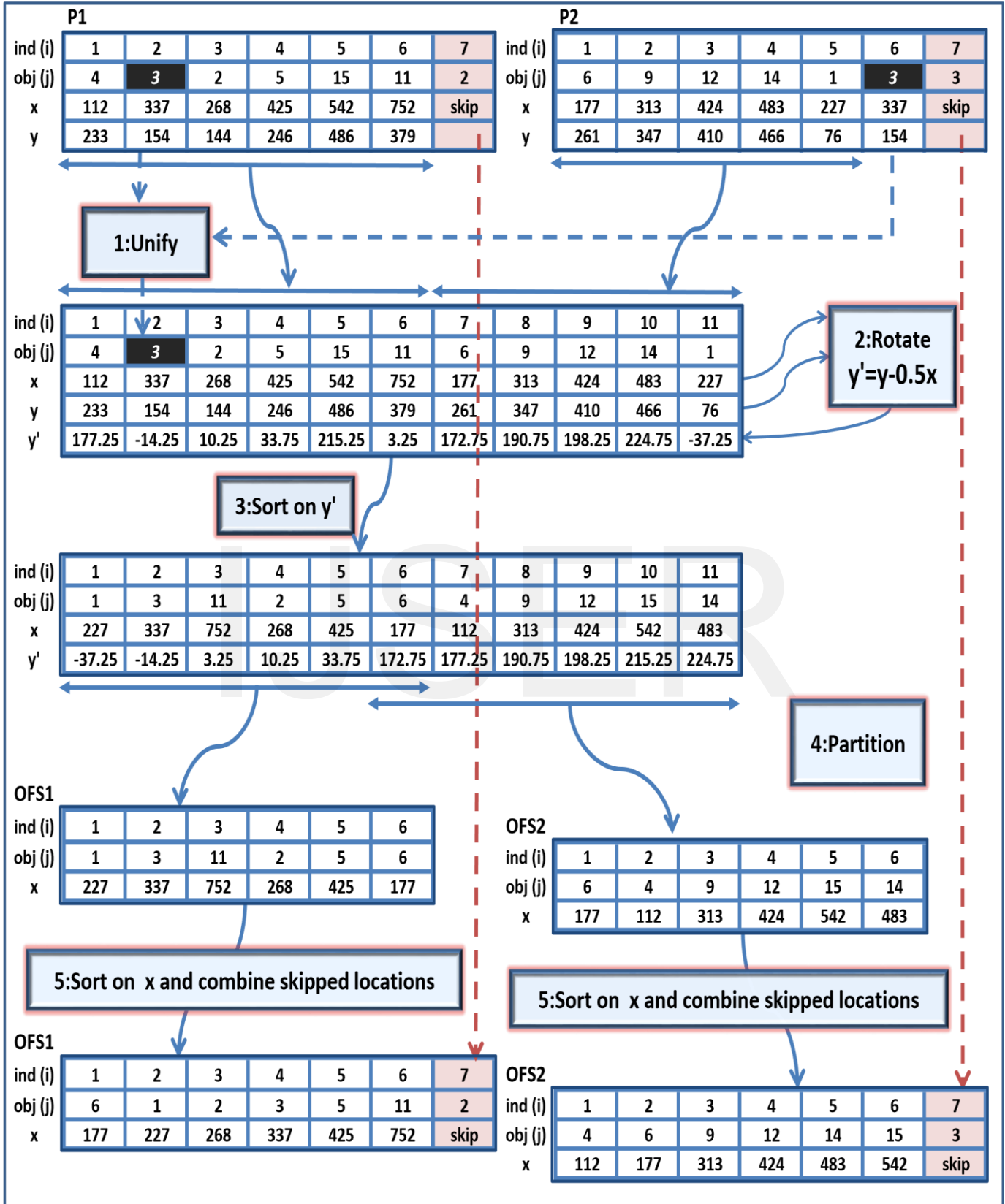


Fig. 8. The steps of the URSPS crossover operator. The slope and y-coordinates are inverted because the positive Y-axis in MATLAB figures points downward.

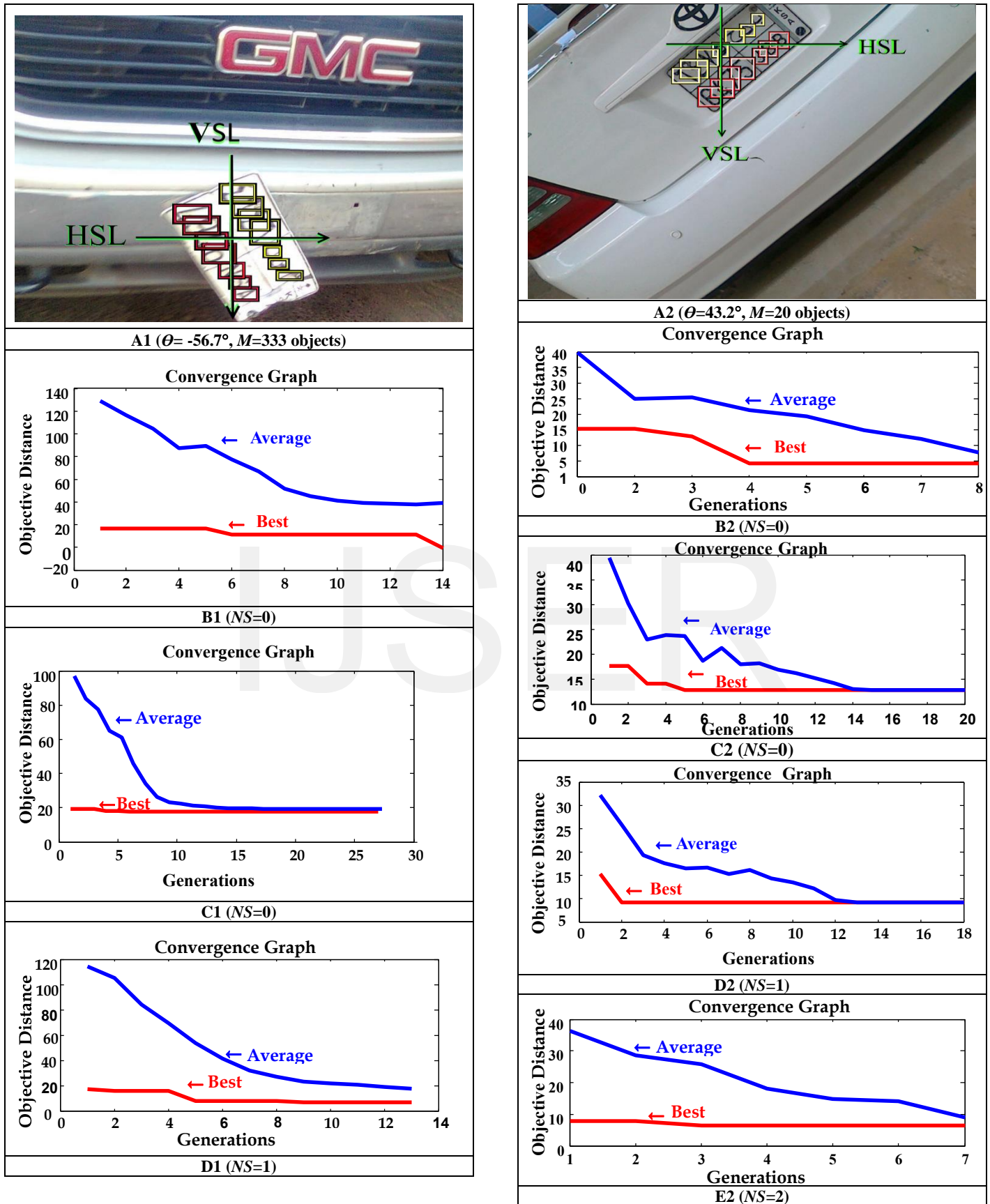


Fig. 9. Convergence graphs for two different LP images (A1 and A2) using the new URSPS at the top graphs (B1 and B2) and the old USPS at the bottom graphs ((C1, D1) for A1 and (C2, D2, E2) for A2).

Although the Latin dataset in [18] was used in testing the system in [3] in conjunction with a Saudi LP dataset, we preferred to do our experiments on the Saudi layout only because it has two number sequences (Arabic and Latin) which always have overlapping problem in case of inclined plates. The Arabic sequence part is considered in our experiment as an interfering part that should be separated from the Latin sequence in the detection process. Another reason for not using the Latin database is the lack of highly inclined samples in it. To the best of our knowledge, a public data set that has the challenging variability of the plate angles in conjunction with other difficulties has not been published until writing this text. This is because most researchers base their proposed solutions on the traditional use of the LP detection problem. Another reason is due to privacy concerns, which prevent most of them from publishing LP images. The lack of a common evaluation database makes evaluations and comparisons with other techniques unfair. Hence, to prove the significance of the new enhancements we focus on the comparison with the previous system developed in [3]. Two experiments have been carried out. The first is carried out on the 1500 test samples using the old system in [3] with a value of 8 for the ODT (now OD_{max}) threshold and a range from -85° to 85° for the GABOSIL-VPN system. The new system is tested twice: the first, without the fake detection stage (NW) and the second using the fake detection stage (NWFD). Each image is tested three times in this experiment leading to a total number of tests (NT) equal to 4500. The second experiment is carried out only on the 48 images shown in Table 4 with the same conditions in the first experiment but each image is tested 10 times leading to 480 tests. The purpose of the second experiment is to test the performance of the GA when faced with a relatively uniform distribution of plate angles along the full range (from -85° to 85°). The results of the two experiments are shown in Table 5.

From both experiments, we notice the following:

















































The previous system failed in the detection of most of the plates having angle ranges from 30° to 85° and from -85° to -30° due to the inability of reaching to the optimum solution using the old crossover in addition to the high objective distance (>8) based on the single horizontal template. Moreover, the selected value (8) of OD_{max} caused the old system to fall into local minima in most cases and hence increased FPs in both experiments. In some cases, the old system overcome the situation in the further runs of the GA where skipping some symbols and keeping non-overlapped ones decreased the OD in these situations.

In case of GABOSIL without fake detection, we got less FPs and less FNs than those produced by the old system but both are still high because of the unexpected inclined fakes that appeared at high angles. For example, at an angle of 80° , OD_{max} reaches 12, which is greater than the ODT (8) of the old system. This allowed some unexpected fakes to be detected as LP symbols as noted from the results at the second row. From the fifth and sixth rows, we can realize the significance of the fake detection stage where we got 0.4%NT as FNs and 1.7%NT as FPs in the second experiment instead of 1.7%NT as FNs and 7.9%NT as FPs without fake detection. Decreasing FPs is expected because most fakes get large HOD (more than 4.5) when

made horizontal. On the other hand, some LP samples may have OD more than OD_{max} but when made horizontal they get very low HOD (less than or equal to 3.5) which transforms their results from FNs to true positives (TPs) and hence the FNs are reduced.

Considering Table 4, various examples of images detected by GABOSIL-VPN system are presented with their angles (1st value) and OD values under each image. The 2nd value represents OD for [3] which is always higher than the 3rd value that represents OD for GABOSIL without fake detection. A value higher than 8 for the 2nd value means that the sample is not detected by [3] at the shown NS (The 5th value). The 4th value represents HOD for GABOSIL with fake detection which is almost lower than the 3rd value. For the sake of fair comparisons, the old OD values shown under each image are measured in the two experiments in the context of the new system (GABOSIL) by fixing the chromosome angle θ_k to 0° when substituting in the GRM which resulted in different values other than announced in [3]. The reason behind this difference is that the template of the new system at 0° differs slightly from the single template in [3] and the objective function weights are slightly different as stated earlier. It should be noted that bold numbers are intended to indicate cases where OD is above the accepted threshold value of the concerned system (8 for [3] and OD_{max} evaluated by (21) for GABOSIL). The success of detecting LPs in the full range from -85° to $+85^\circ$ shown in all rows from A to H demonstrates the ability of the new system to detect plates captured in emergent conditions such as accidents and crime circumstances (obviously within the reported angle range). Getting accuracy above 97% in the performance test in the context of the new wider-angle scope is due to the introduced features in GABOSIL that minimize both FPs and FNs. The first feature that makes GABOSIL highly stable is due to the introduced crossover USPS and its enhanced version URSPS, which guide the search space fast and accurately to the required solution and hence minimize both FPs and FNs as proved in the experiments. The second feature is due to the introduction of the fake detection stage that minimizes both FPs and FNs by pushing the GA to try another solution in case of fakes or FNs with more skipping which allows it to recover from the previous local minima. Moreover, decreasing the problem dimensionality in case of skipping from $Z \times (L+NS+1)$ to $Z \times L$ by the new compact implementation increases the probability of getting the required solution and consequently increases the speed and ability of GABOSIL when recovering from local minima. In addition, penalizing the OD thresholds in case of skipping by multiplying them by $(L-NS)/L$ increases the accuracy and stability of the GA by making the skipping more controllable. Finally, calculating the OD of each chromosome based on its corresponding inclined prototype (in the multidimensional GRM) minimizes its value and makes the unknown inclined plate chromosomes dominate the search space which results in more TPs and less FPs.

TABLE 4: IMAGES TESTED IN EXPERIMENT 2 WITH VALUES OF ANGLES, *OD* (OLD), *OD* (NW), *HOD* (NWFD), AND *NS* UNDER EACH IMAGE. WHERE DETECTED SYMBOLS IN THE LATIN PART ARE OUTLINED BY RED DOUBLE-LINE RECTANGLES AND SKIPPED ONES ARE OUTLINED BY BLUE SINGLE-LINE RECTANGLES. THE ARABIC PART IS OUTLINED BY A SEMI-AUTOMATIC METHOD BASED ON THE LATIN PART GEOMETRY TO INDICATE THE OVERLAPPING OBJECTS.

A						
DATA	5/3.37/2.96/3.56/0	5/2.1 /0.90/0.9/1	22/8.9 /2.79/1.7/1	23/12.4/4 45/2.65/0	-19/7.39/1.2/1.2/3	-24/10.51 /5.2/4.5/1
B						
DATA	12/5.46/2.27/2.27/0	14/8.54/4.08/3.08/0	-12/4.11/1.6/1.6/0	-15/8.63/3.07/2.5/0	-16/7.81/3.02/2.5/2	-19/7.29/3.05/1.5/0
C						
DATA	-10/3.41/1.15/1.67/0	-14/5.19/2.98/2.2/0	-15/5.572.4/1.62/0	-19/5.9/2.01/1.3/0	-23/7.29/5.29/3.3/0	-23/8.13/3.4/2.4/0
D						
DATA	-25/7.29/3.69/2.1/0	-26/8.7/2.3/1.7/0	-31/8.57/5.5/2.6/0	-35/10.3/2.52/1.1/0	-43/11.3/7.6/2.9/0	-44/13.8/2.4/1.0/0
E						
DATA	3/1.86/1.51/1.7/0	11/4.41/2.9/2.7/0	13/4.5/1.79/1.4/0	17/5.56/2.39/1.3/0	19/6.46/3.12/1.8/0	27/8.63/1.5/0.77/3
F						
DATA	28/8.24/4.52/2.4/0	30/8.66/2.55/1.3/0	33/9.19/4.96/3.3/0	38/11.44/3.7/2.2/0	42/11.22/3.3 /2.3/0	43/12.31/3.5/1.9/0
G						
DATA	-46/20/10.1/2.1/0	-49/14.3/2.7/1.8/0	-56/20.4/5.2/2.4/0	-65/21.2/7.0/2.3/0	-73/29.7/7.4/1.8/0	-85/30.7/4.0/1.5/0
H						
DATA	47/12.4/5.95/2.8/1	48/14.9/3.75/2.8/0	62/25.5/10.7/1.7/0	68/18.2/7.02/4.3/0	73/23.4/4.09/1.5/0	85/32.35/2.6/2.7/0

Considering the total performance of the genetic phase, many improvements have been introduced to compensate for the overhead of the new enhancements done in the URSPS crossover operator and the objective function evaluation. As mentioned before we have added new filtering stages to minimize the number of output objects (M) and changed the chromosome and the GRM layouts to speed up the computation in the GA phase. Due to the performed compensation enhancements, the average detection time measured on the same PC (2.6 GHZ with 2 GB RAM) used in [3] remains the same for slightly inclined plates while it is increased by 10% in case of highly inclined plates leading to about 0.13s to locate the LP symbols for low resolution images (640x480) and 0.37s for high resolution images (2048x1536).

TABLE 5: THE RESULTS OF THE 1ST AND 2ND EXPERIMENTS WHERE ALL PERCENTAGES ARE CALCULATED BASED ON THE TOTAL NUMBER OF TESTS IN THE SECOND COLUMN.

Exp.	Number of tests (NT)	Detected		FNs# (%)	FPs# (%)
		without skipping	with skipping		
1 st (OLD)	1500x3	3414	270	438 (9.7%)	378 (8.4%)
1 st (NW)	1500x3	3849	459	39 (0.9%)	153 (3.4%)
1 st (NWFD)	1500x3	3795	624	22 (0.5%)	59 (1.3%)
2 nd (OLD)	48x10	193	74	125 (26%)	88 (18.4%)
2 nd (NW)	48x10	365	69	8 (1.7%)	38 (7.9%)
2 nd (NWFD)	48x10	405	65	2 (0.4%)	8 (1.7%)

If we consider all the techniques mentioned in [1] and [2], we will be convinced that our system localization time is comparable to the recorded times for the detection (the major bottleneck in the processing time in the ALPR problem) and segmentation steps where the minimum time is 0.03s and the maximum is 3.2s using different test images with resolution that ranges from 320 × 240 to 800 × 600 (maybe there are larger sizes but not explicitly written), we will recognize that most reported real times are for small sizes such as 320x240. Hence, we can conclude, assuming linear relationship between the detection time and the image size, that our system can detect the smallest LP (with size equal to 320 × 240) in 0.12/4 (=0.03s). Another important criteria that should be taken into consideration when comparing GABOSIL with other techniques is the scope of each variable in the detection problem. Having a wider scope of the problem variables affects the system performance (relative to other application-based systems) when applied on a narrower context. Stressing the fact that our technique has a wider scope than almost all the techniques mentioned in [1] and [2] in both scale and orientation makes it a promotable competitor in the LP detection domain. However, further filtering and clustering of objects and analysis of the system speed are required to improve its performance and capabilities. On the other hand, further studies can consider comparisons in speed and stability

with other evolutionary techniques or bio-inspired algorithms that may compete in solving the LP detection problem. Experimentally, the enhanced system proved more ability to detect plates in pictures taken in emergent circumstances that do not allow adjustment of the position and orientation of the camera with respect to the vehicle. In spite of increasing the complexity of the system, the new enhancements increase the system ability to cope with complex situations and reduce human intervention rate by minimizing the system failure rate in the detection of inclined LPs at a wider range of angles.

7 CONCLUSION

An enhancement of the previously designed genetic based prototype system for localizing 2-D compound objects inside plane images has been introduced to support the detection of severely inclined LPs. A higher level of flexibility has been introduced in the USPS crossover operator to allow separation of inclined license numbers resulting in the enhanced URSPS operator that can separate linearly separable objects sequences instead of only vertically or horizontally separable objects in the case of the original USPS operator. An efficient layout of the chromosome has been introduced to model the skipped and non-skipped symbols of the license plates. Moreover, the layout of the GRM is evolved to support fast and efficient objective distance evaluation in case of skipped symbols and inclined plates by storing shift and scale invariant geometric relationship values at every relevant direction in the specified angle range. Minimization of both FPs and FNs has been achieved by the addition of the fake detection stage that transforms the GA output to the most stable and suitable orientation (horizontal) for deciding its validity. Another minor but very important addition is the detection of the angle of inclination of the plate, which will support the final step in the ALPR system (character recognition step). Finally, fine-tuning of the objective distance function and its thresholds has been done by changing the weighting parameters and adding factors that incorporate the inclined plate angle and the number of skipped symbols. The results were encouraging showing increased ability of the new system in the detection of license plates in complex geometrical situations. Although our approach has an acceptable speed and accuracy besides its superiority in scale and orientation, more research effort is still needed to cover not only in-plane rotation but also all types of perspective distortion and to allow for the detection of multiple plates and even multiple styles in the same image. In addition, image processing cards and techniques of pipelining and parallel processing can be used to enhance the performance of the system and hence apply it in real time monitoring applications that require faster speed with higher resolution images. Finally, the enhanced system can be used as a general solution based on GA to detect compound objects in complex environments.

Appendix

A TABLE OF BILINGUAL, TWO LINE AND SINGLE LINE LPs (FOR DIFFERENT COUNTRIES) IN WHICH INTERFERING OBJECTS REQUIRE THE APPLICATION OF THE NEW URSPS CROSSOVER IN THE GA PHASE.

Virginia	Arizona	California	INDIANA	Canada-Ontario
Croatia	Croatia	Croatia	Croatia	Croatia
Greece	Greece	Greece	Greece	Greece
Argentina	Brazil	Mexico	PARAGUAY	Colombia
Indonesia	Cambodia	Nigeria	Liberia	Thailand
Egypt	Sudan	Albahrain	Libanon	Qatar

ACKNOWLEDGMENT

The author wishes to thank all the FCIT members in King Abdulaziz University, specially the Dean and the Head of CIS department for the facilities provided to complete this research.

REFERENCES

- [1] S. Du, M. Ibrahim, M. Shehata, and W. Badawy, "Automatic license plate recognition (ALPR): A state-of-the-art-review," *IEEE Trans. Circ. Sys. Video Tech.*, vol. 23, pp. 311-325, Feb. 2013.
- [2] D. Gilly and K. Raimond, "A survey on license plate recognition systems," *International Journal of Computer Applications*, vol. 61, no. 6, pp. 34-40, 2013.
- [3] G. Abo Samra, F. Khalefeh, "Localization of License Plate Number Using Dynamic Image Processing Techniques and Genetic Algorithms," *IEEE Trans. Evolutionary Computation*, vol.18, pp. 244-257, April, 2014.
- [4] P. Tarabek, "Fast license plate detection based on edge density and integral edge image," in *Proc. Int. Conf. Appl. Mach. Intell. Inform.*, 2012, pp. 37-40. doi:10.1109/SAMIL.2012.6208994
- [5] S. K. Kim, D. W. Kim, and H. J. Kim, "A recognition of vehicle license plate using a genetic algorithm based segmentation," in *Proc. Int. Conf. Image Process.* 1996, vol. 1, pp. 661-664.
- [6] J. Xiong, S. Du, D. Gao, and Q. Shen, "Locating car license plate under various illumination conditions using genetic algorithm," in *Proc. ICSP*, 2004, vol. 3, pp. 2502-2505.
- [7] Z. Ji-yin, Z. Rui-rui, L. Min, and L. Yinin, "License plate recognition based on genetic algorithm," in *Proc. Int. Conf. Comput. Sci. Software Eng.*, Dec. 2008, vol. 1, pp. 965-968.
- [8] K. Simunic, and S. Loncaric, "A genetic search-based partial image matching," in *Proc. ICIPS*, 1998, pp. 119-122.
- [9] H. H. Ammar and Y. Tao, "Fingerprint registration using genetic algorithms." In *Proc. 3rd IEEE Symposium on Application-Specific Systems and Software*

Engineering Technology, 2000, pp. 148-154.

- [10] G. Garai and B. B. Chaudhuri, "A cascaded genetic algorithm for efficient optimization and pattern matching", *Image and Vision Computing*, vol.20, no.4, pp. 265-277, Apr. 2002.
- [11] T. Akashi, Y. Wakasa, K. Tanaka, S. Karungaru, and M. Fukumi, "Using genetic algorithm for eye detection and tracking in video sequence." *Journal of Systems, Cybernetics and Informatics*, vol. 5 no.2, pp. 72-78, 2007.
- [12] R.R. Da Silva, C.R. ERIG LIMA, and H.S. Lopes, "Template matching in digital images using a compact genetic algorithm with elitism and mutation," *Journal of Circuits, Systems, and Computers*, vol. 19, no.01, pp. 91-106, 2010.
- [13] R. Singhai, and J. Singhai, "Registration of satellite imagery using genetic algorithm." In *Proc. WCE*, London, U.K, July 4 - 6, 2012.
- [14] S.A. Malik, R.S. Kunwar, and M.E. Haque, "Automatic image registration using evolutionary algorithm." *Recent Research in Science and Technology* vol.4. no.1 Jan.2012.
- [15] G. Garai, and B.B. Chaudhuri, "A novel hybrid genetic algorithm with Tabu search for optimizing multi-dimensional functions and point pattern recognition." *Information Sciences*, vol. 221, pp. 28-48, Feb. 2013.
- [16] G. Avci, M. K. Mehmet, H. Altun, Fuat K., and A. Mehmet, "Implementation of an hybrid approach on FPGA for license plate detection using genetic algorithm and neural networks," *INISTA /Trabzon*, 2009, pp. 392-396.
- [17] J. Muhammad and H. Altun (2015, Nov), "Intelligent License Plate Detection Using Genetic Algorithm," Presented at ELECO (9th International Conference on Electrical and Electronics Engineering, [Online]. Available: http://www.eleco.org.tr/openconf_2015/modules/request.php?module=oc_proceedings&action=view.php&id=153&a=Accept+as+Poster
- [18] Medialab Web site, (2015, DEC, 9). [Car Images]. Available: <http://www.medialab.ntua.gr/research/LPRdatabase.html>

G. Abo Samra received the B.S., M. Eng., and Ph.D. degree from the faculty of Engineering in Cairo University, Egypt in 1983, 1988, and 1992, respectively, in electronic and communication engineering. He is currently an associate professor at the faculty of Computing and Information Technology, King Abdulaziz University-Saudi Arabia. His research interests include image processing, pattern recognition, genetic algorithms, computer vision, data hiding, OCR, and intelligent transportation systems. Many researches were supported by the Deanship of Scientific Research (DSR), King Abdulaziz University and King Abdulaziz City for Sciences and Technology.

